Excitation energies and transition rates in the $3d^2$ states of Ca-like ions

U. I. Safronova,[1] W. R. Johnson,[1] D. Kato,[2] and S. Ohtani[2,3]
[1]*Department of Physics, University of Notre Dame, Notre Dame, Indiana 46556*
[2]*Cold Trapped Ions Project, ICORP, JST, Choufu, Tokyo 182-0024, Japan*
[3]*University of Electro-communication, Choufu, Tokyo 182-8585, Japan*
(Received 28 July 2000; revised manuscript received 5 October 2000; published 14 February 2001)

Energies, transition probabilities, and lifetimes are calculated for $3d^2$ states in Ca-like ions with nuclear charges Z ranging from 22 to 100. Relativistic many-body perturbation theory (MBPT), including the Breit interaction, is used to evaluate retarded $M1$ and $E2$ matrix elements. The calculations start from a $1s^22s^22p^63s^23p^6$ Dirac-Fock potential. First-order perturbation theory is used to obtain intermediate coupling coefficients and second-order MBPT is used to determine matrix elements. Contributions from negative-energy states are included in the second-order $M1$ and $E2$ matrix elements. The resulting transition energies and lifetimes are compared with experimental values and with results from other recent calculations.

DOI: 10.1103/PhysRevA.63.032518 PACS number(s): 32.70.Cs, 31.15.Md, 31.25.Jf, 31.30.Jv

I. INTRODUCTION

Levels in the $3d^2$ ground-state multiplet along the calcium isoelectronic sequence have been observed experimentally for ions with nuclear charge $Z \geqslant 22$. In three NIST publications, energy levels of the $3d^2$ configuration were reported for Ti^{2+}-Mn^{5+} [1], Fe^{6+}-Ni^{8+} [2], and Cu^{9+} [3]. These energies were obtained by classifying the spectral lines associated with electric-dipole transitions from low-lying excited odd configurations $3p^53d^3$, $3p^63d4p$, and $3p^63d4f$ to the ground-state configuration $3p^63d^2$.

Magnetic-dipole transitions between $^3F_3$ and $^3F_2$ levels of the $3d^2$ configuration for Fe^{6+}-Ni^{8+}, Zr^{20+}, and Mo^{22+} were identified by Edlén in Ref. [4]. Forbidden lines were also observed in several nebulae and hot stars. Among these, the slow nova RR Telescopii was investigated by Thackeray [5], who gave accurate spectroscopic data collected during the period 1951-1973. A detailed analysis of the $3d^2$ forbidden transitions in Fe^{6+} was given by Ekberg in Ref. [6], where wavelengths and intensities of the 17 forbidden transitions within the $3d^2$ multiplet were predicted and compared with Thackeray's line list. The $3d^2$ level structure in Fe^{6+} was interpreted theoretically in Ref. [6] and energy parameters, determined from least-squares fits to the observed levels, were compared with Hartree-Fock calculations. Ekberg also calculated magnetic dipole (M1) and electric quadrupole (E2) transition probabilities using the Cowan code [7]. Altogether, Ekberg [6] identified 11 stellar lines from Thackeray's line list as forbidden transitions within $3d^2$ ground-state multiplet in Fe^{6+}.

One of the first calculations of the $3d^2$ energy levels and forbidden transition probabilities within the $3d^2$ configuration was presented by Warner and Kirkpatrick [8] who derived empirical Slater parameters from a study of energy levels in the isoelectronic sequence Ti^{2+}-Ni^{6+}. Energy matrices were constructed using the Cowan code and line strengths for $M1$ and $E2$ radiation were evaluated in Ref. [8] using scaled Thomas-Fermi wave functions. Nussbaumer and Storey [9] also calculated wavelengths and $M1$, $E2$ transition probabilities for the 27 transitions between the nine $3d^2$ levels ^3F_J, $^1D_2$, ^3P_J, $^1G_4$, and $^1S_0$ in Fe^{6+} using radial wave functions obtained from a combination of screened hydrogenic and scaled Thomas-Fermi potentials. Parametric studies of the $3d^2$ ground configuration in highly-charged ions were presented by Wyart *et al.* in Ref. [10], where the parameters needed for an accurate interpretation of the $3d^2$ configuration within the framework of the Slater-Condon theory were determined using a generalized least-squares technique. The intermediate coupling eigenvalues and eigenfunctions obtained in Ref. [10] were used to calculate $M1$ transition probabilities within the $3d^2$ multiplet in Co^{7+}, Ni^{8+}, Ge^{12+}, Se^{14+}, Zr^{20+}, Mo^{22+}, and Ag^{27+}. More recent calculations of $M1$ and $E2$ transition probabilities were given by Biémont *et al.* [11] for the ions Ti^{3+} to Ag^{17+} using three different computer programs: the (HFR) code of Cowan [7], the Multiconfiguration Dirac-Fock (MCDF) code of Grant *et al.* [12], and the code SUPERSTRUCTURE (SST) of Eissner *et al.* [13], in the version due to Nussbaumer and Storey [14]. These three different methods of taking configuration interaction into account were compared in Ref. [11] with respect to their ability to predict energy levels and transition probabilities within the $3d^2$ configuration. Two configurations $4d^2$ and $4f^2$ were added to the HFR calculations in addition to the nine configurations ($3d^2$, $3s4s$, $3d4d$, $4s^2$, $4p^2$, $4s4d$, $4p4f$, $3d5s$, and $3d5d$) used in the MCDF calculations of Ref. [11]. The HFR method was found to be well-suited to low and medium ionization stages while MCDF method was judged superior for highly-charged ions where relativistic effects become important [11]. These conclusions, of course, depend on the choice of configurations.

In the present paper, relativistic many-body perturbation theory (MBPT), including the Breit interaction, is used to evaluate retarded $M1$ and $E2$ matrix elements. Second-order MBPT using a Dirac-Fock basis allows one to consider correlation effects directly by summing over virtual states. This method has been used recently to obtain accurate excitation energies and transition rates in Be-like [15–20], B-like [21,22], and in Mg-like [23] ions for a wide range of Z. Our calculations start from a $1s^22s^22p^63s^23p^6$ Dirac-Fock potential. First-order MBPT is used to obtain intermediate cou-

TABLE I. Possible states in the $3d^2$ multiplet.

jj coupling	*LS* coupling	*jj* coupling	*LS* coupling	*jj* coupling	*LS* coupling
$3d_{3/2}3d_{3/2}(0)$	$3d^2\,{}^3P_0$	$3d_{3/2}3d_{3/2}(2)$	$3d^2\,{}^3F_2$	$3d_{3/2}3d_{5/2}(3)$	$3d^2\,{}^3F_3$
$3d_{5/2}3d_{5/2}(0)$	$3d^2\,{}^1S_0$	$3d_{3/2}3d_{5/2}(2)$	$3d^2\,{}^1D_2$	$3d_{3/2}3d_{5/2}(4)$	$3d^2\,{}^3F_4$
$3d_{3/2}3d_{5/2}(1)$	$3d^2\,{}^3P_1$	$3d_{5/2}3d_{5/2}(2)$	$3d^2\,{}^3P_2$	$3d_{5/2}3d_{5/2}(4)$	$3d^2\,{}^1G_4$

pling coefficients and second-order MBPT is used to determine matrix elements. The transition energies used in the calculation of transition rates are evaluated using second-order MBPT. Contributions from negative-energy states are included in second-order $M1$ and $E2$ matrix elements. Excitation energies, transition probabilities, and lifetimes are evaluated for all states in the $3d^2$ ground-state multiplet for Ca-like ions with nuclear charges Z from 22 to 100.

II. THEORETICAL TECHNIQUE

The MBPT formalism developed previously [15–23] for ions with two valence electrons is used here to obtain second-order energies and to evaluate first- and second-order transition matrix elements in Ca-like ions. Differences between the present calculations and previous MBPT calculations for Be-like and Mg-like ions are primarily due to the model space ($3d3d'$ instead of $2l2l'$ or $3l3l'$) and the Dirac-Fock potential ($1s^22s^22p^63s^23p^6$ instead of $1s^2$ or $1s^22s^22p^6$). These differences lead to lengthier numerical calculations.

A. Model space

The model space for the $3d^2$ complex in Ca-like ions consists of nine even-parity states. These states are summarized in Table I where both *jj* and *LS* designations are given. When starting calculations from relativistic Dirac-Fock wave functions, it is natural to use *jj* designations for uncoupled transition and energy matrix elements; however, neither *jj* or *LS*-coupling describes *physical* states properly, except for the two single-configuration states $3d_{3/2}3d_{5/2}(1)\equiv 3d^2\,{}^3P_1$ and $3d_{3/2}3d_{5/2}(3)\equiv 3d^2\,{}^3F_3$.

Strong mixing between $3d_{3/2}3d_{5/2}(J)$ and $3d_{5/2}3d_{5/2}(J)$ states with $J=2$ or 4 leads to rapid variations with Z in the Grotrian energy diagram. The variation of the $3d^2$ levels from $Z=22$ to $Z=27$ was shown by Ekberg [6]; however, it was not evident from Ref. [6] that the ${}^1D_2$ level could cross the ${}^3F_J$ and ${}^3P_J$ levels. These level crossings are shown in Fig. 1 where energies relative to the ${}^3F_2$ state are shown as functions of Z. It is seen that levels ${}^1D_2$ and ${}^3P_0$ cross for $Z=38-39$, levels ${}^1G_4$ and ${}^3P_2$ cross for $Z=42-43$, and levels ${}^1D_2$ and ${}^3F_4$ cross for $Z=50-52$. The energy diagram changes drastically in the interval $Z=38-52$. In this interval neither *jj* or *LS* coupling describes *physical* states. For small Z ($Z=22-38$), it is reasonable to use the *LS* coupling scheme, while for high Z ($Z>52$), the *jj* coupling scheme is preferable. Both designations are shown in Fig. 1: *LS* for low Z and *jj* for high Z.

B. Excitation energy

Details of the theoretical method used to evaluate second-order energies for Ca-like ions have been presented previously in Ref. [15] for Be-like ions and will not be repeated here. The energy calculations are illustrated in Table II, where we list contributions to the energies of the $3d^2$ levels relative to the $1s^22s^22p^63s^23p^6$ core and energies relative to the $3d^2\,{}^3F_2$ level in Fe^{+6} from zeroth- plus first-order Coulomb and Breit energy $E^{(0+1)}=E^{(0)}+E^{(1)}+B^{(1)}$ and from the second-order Coulomb energy $E^{(2)}$. We also give the total theoretical energy $E^{(\mathrm{tot})}$. As can be seen, the second-order contribution is about 3% of the total energy but is from 10% to 30% of the excitation energy. This table shows clearly the importance of including second-order contributions. In Fig. 2, we show the Z-dependence of the $E^{(2)}$ corrections given in Table II. As can be seen from this figure, the second-order energy $E^{(2)}$ slowly increases with Z and is in the range $6-10\times 10^4$ cm^{-1}.

C. Electric quadrupole transitions

We designate the first-order quadrupole matrix element by $Z^{(1)}$, the Coulomb correction to the second-order matrix element by $Z^{(2)}$, and the second-order Breit correction by $B^{(2)}$. A detailed discussion of the first-order quadrupole matrix element is given in Appendix A. The evaluation of $Z^{(2)}$ and $B^{(2)}$ for Ca-like ions follows the pattern of the corresponding calculation for Be-like ions given in Ref. [19].

The quadrupole matrix elements are calculated in both length (L) and velocity (V) forms. The differences between L and V forms, are illustrated for the uncoupled $3d_{3/2}3d_{3/2}(0)-3d_{3/2}3d_{5/2}(2)$ matrix element in Fig. 3. In the Coulomb approximation, the first-order matrix element $Z^{(1)}$

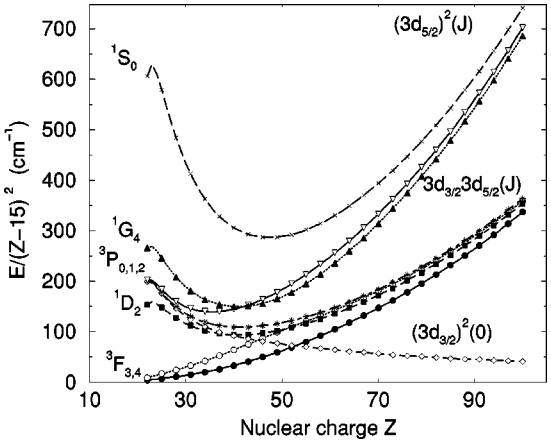

FIG. 1. Z-dependence of the $3d^2$ energy levels.

TABLE II. Energy of $3d^2$ states in Ca-like Fe^{6+} (cm^{-1}). Notation: $E^{(0+1)}=E^{(0)}+E^{(1)}+B^{(1)}$.

Level	$E^{(0+1)}$	$E^{(2)}$	$E^{(\mathrm{tot})}$	$E^{(0+1)}$	$E^{(2)}$	$E^{(\mathrm{tot})}$
	Absolute values			Relative to the ground state		
$^3F_2$	−2167903	−67912	−2235815	0	0	0
$^3F_3$	−2167003	−67767	−2234771	900	144	1044
$^3F_4$	−2165886	−67604	−2233490	2018	308	2325
$^1D_2$	−2145951	−72810	−2218761	21952	−4898	17054
$^3P_0$	−2142507	−73372	−2215879	25396	−5460	19936
$^3P_1$	−2142182	−73309	−2215491	25721	−5397	20324
$^3P_2$	−2141524	−73151	−2214675	26379	−5240	21140
$^1G_4$	−2134356	−73319	−2207675	33547	−5407	28140
$^1S_0$	−2086112	−83637	−2169750	81791	−15726	66065

is proportional $1/Z^2$, the second-order matrix element $Z^{(2)}$ is proportional $1/Z^3$, and the second-order Breit matrix element $B^{(2)}$ is proportional $1/Z$ (see Ref. [18]). These Z dependencies apply to second-order matrix elements $Z^{(2)}$ and $B^{(2)}$ calculated in length form only.

The contribution of the second-order matrix elements $Z^{(2)}$ and $B^{(2)}$ is much larger in V form as can be seen by comparing the upper and lower panels in Fig. 3. The differences between L and V forms shown in Fig. 3 are compensated by ''derivative'' terms $P^{(\mathrm{derv})}$. It should be noted, that $P^{(\mathrm{derv})}$ in V form almost equals $Z^{(1)}$ in V form; whereas $P^{(\mathrm{derv})}$ in L form is about two times larger than $Z^{(1)}$ in L form. The cusp in the L-form matrix element $Z^{(2)}$ in the lower panel of Fig. 3 (absolute values are shown in the figure) is caused by cancellation of random-phase approximation (RPA) $Z^{(\mathrm{RPA})}$ and correlation $Z^{(\mathrm{corr})}$ diagrams, each of which is a smooth function of nuclear charge Z.

Physical two-particle states are linear combinations of uncoupled two-particle states (vw) in a model space having fixed values of angular momentum and parity; consequently, the transition amplitudes between physical states are linear combinations of the uncoupled transition matrix elements such as those shown in Fig. 3. The expansion coefficients and energies are obtained by diagonalizing the effective Hamiltonian as discussed in Ref. [15]. The first-order expansion coefficient $C_1^{\lambda}(vw)$ is the λth eigenvector of the first-order effective Hamiltonian, and E_1^{λ} is the corresponding eigenvalue. In the present calculation, both Coulomb and Breit interactions are included in the first-order effective Hamiltonian. The coupled transition amplitude between the Ith, initial eigenstate, which has angular momentum J, and the Fth final state, which has angular momentum J', is given by

$$T[I-F]=\sum_{vw}\sum_{v'w'} C_1^I(vw)C_1^F(v'w') \times\{T^{(1+2)}[vw(J)-v'w'(J')] +T^{(\mathrm{derv})}[vw(J)-v'w'(J')]\}. \quad (2.1)$$

In this equation,

$$T^{(1+2)}[vw(J)-v'w'(J')] =[\epsilon_{vw}-\epsilon_{v'w'}][Z^{(1+2)}[vw(J)-v'w'(J')] +B^{(2)}[vw(J)-v'w'(J')]],$$

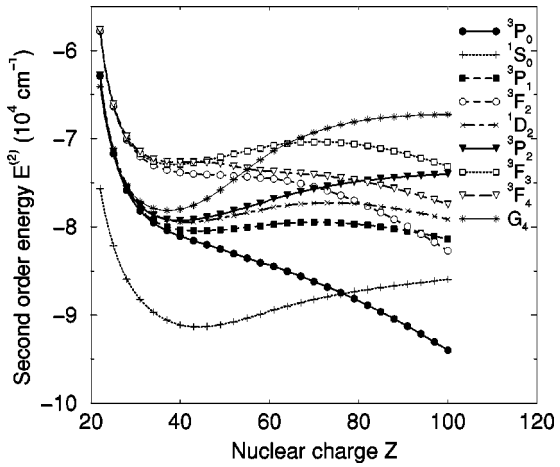

FIG. 2. Z-dependence of the second-order energy for the $3d^2$ energy levels.

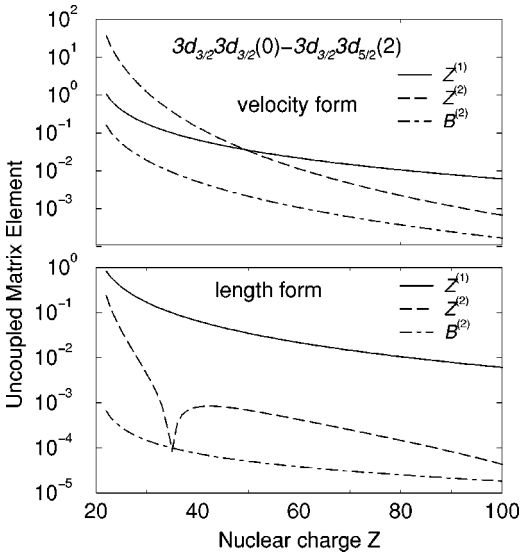

FIG. 3. Uncoupled matrix element for $3d_{3/2}3d_{3/2}(0)-3d_{3/2}3d_{5/2}(2)$ calculated in length and velocity forms.

$$T^{(\mathrm{derv})}[vw(J)-v'w'(J')] = [E_1^I-E_1^F-\epsilon_{vw}+\epsilon_{v'w'}]P^{(\mathrm{derv})}[vw(J)-v'w'(J')], \tag{2.2}$$

where $\epsilon_{vw}=\epsilon_v+\epsilon_w$ and $Z^{(1+2)}=Z^{(1)}+Z^{(\mathrm{RPA})}+Z^{(\mathrm{corr})}$. Using these formulas and numerical results for uncoupled reduced matrix elements, we transform from uncoupled reduced matrix elements to intermediate coupled reduced matrix elements between physical states.

A qualitative difference between the $E2$ transitions studied here and the $E1$ transitions studied previously in Refs. [18,19] is that $E2$ transitions can occur between states with $vw=v'w'$ while the corresponding $E1$ transitions are forbidden. In such cases

$$T^{(1+2)}[vw(J)-vw(J')]=0,$$
$$T^{(\mathrm{derv})}[vw(J)-vw(J')] = [E_1^I-E_1^F]P^{(\mathrm{derv})}[vw(J)-vw(J')]. \tag{2.3}$$

It was already mentioned that the value of $P_L^{(\mathrm{derv})}$ in length form is larger by a factor of 2 than the value of $P_V^{(\mathrm{derv})}$ in velocity form. As a result, there are huge differences between transition amplitudes calculated in length and velocity forms. These differences are compensated by the velocity form of the second-order diagram $Z^{(\mathrm{corr})}$ discussed in Appendix B:

$$Z^{(\mathrm{corr})}[vw(J)-vw(J')] = \frac{1}{\omega}[E_1^I-E_1^F]P_V^{(\mathrm{derv})}[vw(J)-vw(J')], \tag{2.4}$$

where

$$P_V^{(\mathrm{derv})}[vw(J)-vw(J')] = \sqrt{[J][J']}(-1)^{j_v+j_w}\left[Z(vv)(-1)^J\begin{Bmatrix} J & J' & 2 \\ j_v & j_v & j_w \end{Bmatrix} + Z(ww)(-1)^{J'}\begin{Bmatrix} J & J' & 2 \\ j_w & j_w & j_v \end{Bmatrix}\right]. \tag{2.5}$$

As a result, we obtain an additional contribution to the transition amplitude in velocity form:

$$T^{(1+2)}[vw(J)-vw(J')] = [E_1^I-E_1^F]P_V^{(\mathrm{derv})}[vw(J)-vw(J')]. \tag{2.6}$$

The above contribution completely compensates the difference between transition amplitudes calculated in length and velocity forms for vw(J)-vw(J′) transitions. Let us confirm this conclusion for the transition $3d_{3/2}3d_{5/2}$ (3)-$3d_{3/2}3d_{5/2}$ (1). In this example, both initial and final states are single-configuration states in any coupling scheme. In Table III, we present a breakdown of the contributions for this transition in Ca-like molybdenum. In the first two columns, we compare results obtained with a (local) Coulomb potential in L and V forms. We see that the first-order results and second-order results are identical in the two forms to the six digits quoted. This is true independently for the Coulomb and Breit interactions. We do not obtain precise agreement between L and V forms for the (nonlocal) Dirac-Fock (DF) potential given in the last two columns of the table; however, differences are expected in the DF case since gauge independence is assured only for local potentials. For our example, the $L-V$ difference in T for the DF case is about 0.9%.

TABLE III. Breakdown of the $E2$ coupled reduced matrix element in length (L) and velocity (V) forms for the $3d_{3/2}3d_{5/2}(3)$-$3d_{3/2}3d_{5/2}(1)$ transition in Mo^{22+}. Notation: $T^{(1+2)}=(Z^{(1+2)}+B)[\varepsilon_{vw}-\varepsilon_{v'w'}]$, $T^{(\mathrm{derv})}=P^{(\mathrm{derv})}[E_1^I-E_1^F-\varepsilon_{vw}+\varepsilon_{v'w'}]$.

	(a) Coulomb potential		(b) Dirac-Fock potential	
	L	V	L	V
$T^{(1+2)}$	0	−0.0259635	0	−0.0348475
$T^{(\mathrm{derv})}$	−0.0519270	−0.0259635	−0.0709159	−0.0354578
T	−0.0519270	−0.0519270	−0.0709159	−0.0703053

Let us now show that the transitions $3d^2\,{}^3F_4$-$3d^2\,{}^3F_3$ and $3d^2\,{}^1G_4$-$3d^2\,{}^3F_3$ in Mo^{22+} are gauge independent. For these transitions, the final state $F=3d^2\,{}^3F_3=3d_{3/2}3d_{5/2}(3)$ is a single-configuration state in any coupling scheme and only the initial states are mixed. Using the $[LSJ]$ designation for coupled states $I_1=3d^2\,{}^3F_4$, $I_2=3d^2\,{}^1G_4$, and $[jjJ]$ designations for uncoupled states $3d_{3/2}3d_{5/2}$ (4) and $3d_{5/2}3d_{5/2}$ (4), we can rewrite $T[I_k-F]$ (k distinguishes the two possible initial states) in the following way:

$$\begin{aligned} T[I_k-F] = {} & C_1^{I_k}\{T^{(1+2)}[3d_{3/2}3d_{5/2}(4)-F] \\ & + T^{(\mathrm{derv})}[3d_{3/2}3d_{5/2}(4)-F]\} \\ & + C_2^{I_k}\{T^{(1+2)}[3d_{5/2}^2(4)-F] \\ & + T^{(\mathrm{derv})}[3d_{5/2}^2(4)-F]\}. \end{aligned} \tag{2.7}$$

We list the individual contributions to this transition for Ca-like Mo in Table IV. Results are given for Coulomb and DF potentials. It should be noted, that the $3d_{3/2}3d_{5/2}(4)-3d_{3/2}3d_{5/2}(3)$ transition is treated in the same way as the $3d_{3/2}3d_{5/2}(3)-3d_{3/2}3d_{5/2}(1)$ transition [see Eqs. (2.3)–(2.5)]. In order to avoid divergence in the numerical calculations of $Z^{(\mathrm{corr})}$ in Eqs. (2.4), we set $\omega=10^{-7}$ instead of zero. As can be seen from Table IV, we obtain complete agreement between the results calculated in L and V forms for the Coulomb potential and 1–4% disagreement between L and V results in the DF potential. In a Coulomb potential, even the first-order matrix elements are identical in the two forms for uncoupled matrix elements.

In Fig. 4, we plot the relative difference between line strengths calculated in length form (S_L) and velocity form (S_V) starting from the DF potential. The Z dependence of the ratios $(S_L-S_V)/S_L$ are shown for transitions between $3d^2$

TABLE IV. Contributions to the $E2$ coupled reduced matrix elements in length L and velocity V forms for the $3d^2\,{}^3F_4$-$3d^2\,{}^3F_3$ and $3d^2\,{}^1G_4$-$3d^2\,{}^3F_3$ transitions in Mo^{22+}. Coulomb potential: $E_1^{I_1}-E_1^F=0.016\,854\,059$, $E_1^{I_2}$-$E^F=0.49\,634\,965$, Dirac-Fock potential: $E_1^{I_1}$-$E_1^F=0.109\,942\,927$, $E_1^{I_2}$-$E^F=0.393\,706\,546$, coupled initial states: $I_1=3d^2\,{}^3F_4$, $I_2=3d^2\,{}^1G_4$, uncoupled initial states: (1) $d_{3/2}d_{5/2}[4]$, (2) $d_{5/2}^2[4]$, final state: $3d^2\,{}^3F_3\equiv d_{3/2}d_{5/2}[3]$.

	L	L	V	V
		Coulomb potential		
$T^{(1+2)}(1)$	0	0.0105128	−0.0003958	0.0020645
$T^{(\mathrm{derv})}(1)$	0.0002652	−0.0174613	0.0001326	−0.0087303
C^{I_1}	−0.4716450	−0.8817885	−0.4716450	−0.8817885
$T^{(1+2)}(2)$	0	0.0105128	−0.0003958	0.0020645
$T^{(\mathrm{derv})}(2)$	0.0078087	−0.0008177	0.0039043	−0.0004088
C^{I_2}	−0.8817885	0.4716450	−0.8817885	0.4716450
$T(I-F)$	0.0060020	−0.0231293	0.0060020	−0.0231293
		Dirac-Fock potential		
$T^{(1+2)}(1)$	0	0.0056585	−0.0003759	0.0053814
$T^{(\mathrm{derv})}(1)$	0.0034686	−0.0044301	0.0017445	−0.0022199
C^{I_1}	−0.6437434	−0.7652415	−0.6437434	−0.7652415
$T^{(1+2)}(2)$	0	0.0056585	−0.0003759	0.0053814
$T^{(\mathrm{derv})}(2)$	0.0124210	0.0149155	0.0062469	0.0074742
C^{I_2}	−0.7652415	0.6437434	−0.7652415	0.6437434
$T(I-F)$	−0.0031729	0.0037393	−0.0033003	0.0037829

levels: $^3F_2$-$^3P_0$, $^3F_2$-$^3P_1$, and $^3F_3$-$^3P_1$. As can be seen from the figure, the ratios change slowly with Z and are in the range 1–10%.

D. Magnetic dipole transitions

We evaluate $M1$ amplitudes and line strengths for magnetic dipole transitions in Ca-like ions with nuclear charges $Z=25$, 30, 40, 60, 80, and 100. We find that LS forbidden transitions with $\Delta S=1$ and $\Delta L=2$ become allowed in jj coupling. The $^3F_2$-$^3P_2$ transition has the smallest line strength among the transitions considered; this LS forbidden transition remains forbidden in the jj coupling scheme.

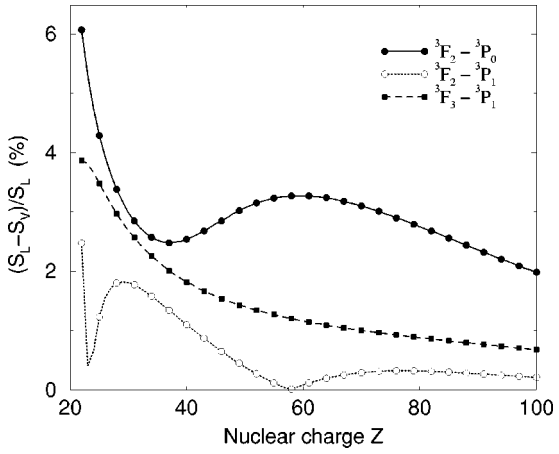

FIG. 4. Z-dependence of the ratio $(S_L-S_V)/S_L$ in % for transitions between $3d^2$ levels.

Negative-energy corrections to $M1$-amplitudes have been recently studied for Be-like ions in Ref. [20]. The leading term for transitions inside the $3d^2$ configuration is of order 1 and arises from the nonrelativistic allowed lowest-order transition. The relative contribution of negative-energy states to the uncoupled magnetic dipole amplitude scales as α^2Z. Consequently, negative energies states contribute less than 1% for transitions between levels of $3d^2$ states. Negative-energy contributions are more important for transitions between different configurations with $\Delta n=1$ [20].

III. RESULTS AND COMPARISONS

We calculated energies of the nine $3d_j3d_{j'}(J)$ excited states for Ca-like ions with nuclear charges ranging from $Z=22-100$. Reduced matrix elements, transition amplitudes, and transition rates are also determined for all 25 allowed and forbidden electric quadrupole and 14 allowed and forbidden magnetic dipole transitions for each ion.

A. Energy levels

In Table V we present energies (cm^{-1}) of states in the d^2 multiplet relative to the $^3F_2$ ground state. Comparisons of these energies with other theoretical and experimental data are too voluminous to include here but are available as supplementary data in Ref. [24]. In Table I of Ref. [24], the energies of Cr^{4+}, Fe^{6+}, and Ni^{8+} are compared with theoretical values from Ref. [11]; the MBPT values are found to agree much better with experimental data. In Table II of Ref. [24], the MBPT results for $3d^2$ excitation energies are compared to recommended data from Refs. [1–3], experimental measurements from [25], and predicted results reported by Wyart *et al.* [10]. Agreement to about 0.01–1% is obtained for most cases. In Table III of Ref. [24], the present MBPT results for fine-structure intervals of the ^3P term are compared with recommended data from Refs. [1] and [2] and found to be in good agreement. It should be mentioned that there are some measurements of fine-structure intervals of the ^3F term in Refs. [4] and [26]. It was proposed by Wyart *et al.* [10], that the line 3319.8 Å measured by Suckewer *et al.* in Ref. [26] should be identified with the $^3P_2$-$^3P_1$ line in Mo^{22+}. Our result for this line is 3357 Å.

B. $M1$ and $E2$ transition rates

Z dependence of $E2$ and $M1$ transition rates for $3d^2LSJ$-$3d^2L'S'J'$ lines in Ca-like ions is shown in Figs. 5–8. In Figs. 5 and 6, we present the $E2$ and $M1$ transition rates for $3d^2\,{}^3P$ and $3d^2\,{}^3F$ multiplets. It should be noted that the energy differences ΔE for the $^3P_2$-$^3P_1$, $^3P_1$-$^3P_0$, and $^3F_3$-$^3F_2$ transitions are proportional to α^2Z^4, but ΔE for the $^3F_4$-$^3F_3$ transition is proportional Z even for high-Z ions. All transitions shown in Figs. 5 and 6 are LS allowed transitions. The line strengths for $E2$ transitions are proportional Z^{-4}, whereas line strengths for $M1$ transitions are almost independent of Z. Taking into account the Z dependence of the line strengths and the relations $A^{E2}\propto S\Delta E^5$ and $A^{M1}\propto S\Delta E^3$, we obtain the following Z dependence for A values;

TABLE V. MBPT energies (cm^{-1}) of $3d^2$ levels relative to $^3F_2$ ground state.

Z	$^3F_3$	$^3F_4$	$^1D_2$	$^3P_0$	$^3P_1$	$^3P_2$	$^1G_4$	$^1S_0$
22	192	439	7473	9771	9840	9961	13 021	29 715
23	328	746	10 184	12 609	12 727	12 945	17 230	40 271
24	510	1151	12 569	15 160	15 344	15 701	21 020	49 442
25	745	1671	14 833	17 578	17 850	18 402	24 619	57 936
26	1044	2325	17 054	19 936	20 324	21 140	28 140	66 065
27	1419	3136	19 275	22 275	22 811	23 976	31 650	74 000
28	1882	4125	21 523	24 621	25 344	26 963	35 198	81 851
29	2447	5318	23 820	26 992	27 952	30 144	38 822	89 697
30	3130	6739	26 186	29 402	30 657	33 562	42 556	97 601
31	3947	8416	28 641	31 863	33 482	37 258	46 435	105 620
32	4916	10 378	31 205	34 384	36 450	41 275	50 490	113 804
33	6056	12 653	33 902	36 972	39 584	45 654	54 755	122 203
34	7390	15 271	36 754	39 634	42 907	50 440	59 266	130 867
35	8939	18 264	39 787	42 376	46 444	55 679	64 060	139 847
36	10 725	21 662	43 027	45 200	50 220	61 417	69 177	149 195
37	12 776	25 495	46 502	48 110	54 262	67 704	74 661	158 966
38	15 115	29 794	50 240	51 105	58 595	74 591	80 559	169 216
39	17 770	34 586	54 272	54 187	63 249	82 130	86 922	180 006
40	20 769	39 898	58 628	57 353	68 253	90 377	93 806	191 398
41	24 142	45 754	63 340	60 601	73 635	99 387	101 272	203 456
42	27 917	52 175	68 440	63 927	79 427	109 219	109 385	216 247
43	32 125	59 180	73 962	67 327	85 660	119 931	118 216	229 839
44	36 797	66 784	79 940	70 795	92 365	131 587	127 845	244 303
45	41 967	74 998	86 407	74 326	99 576	144 247	138 351	259 713
46	47 666	83 833	93 398	77 914	107 326	157 978	149 823	276 141
47	53 928	93 298	100 950	81 553	115 649	172 845	162 352	293 663

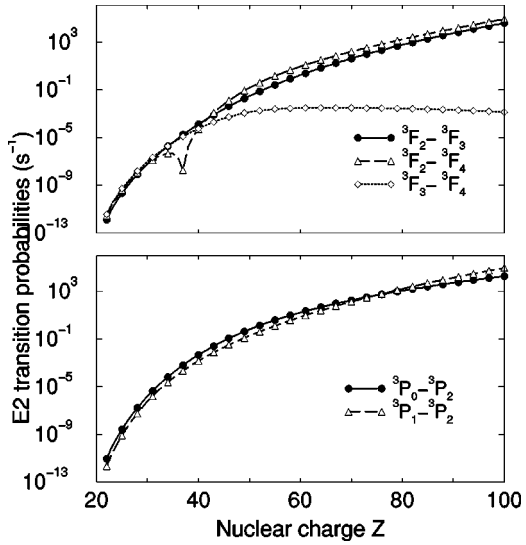

FIG. 5. Transition probabilities for $^3P_J - {}^3P_{J'}$ and $^3F_J - {}^3F_{J'}$ electric quadrupole lines as functions of Z.

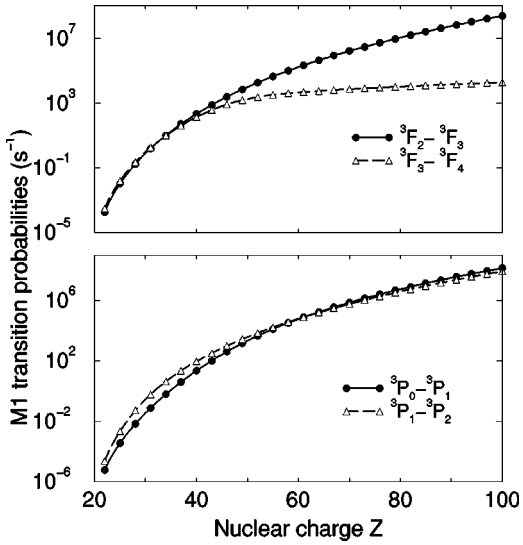

FIG. 6. Transition probabilities for $^3P_J - {}^3P_{J'}$ and $^3F_J - {}^3F_{J'}$ magnetic dipole lines as functions of Z.

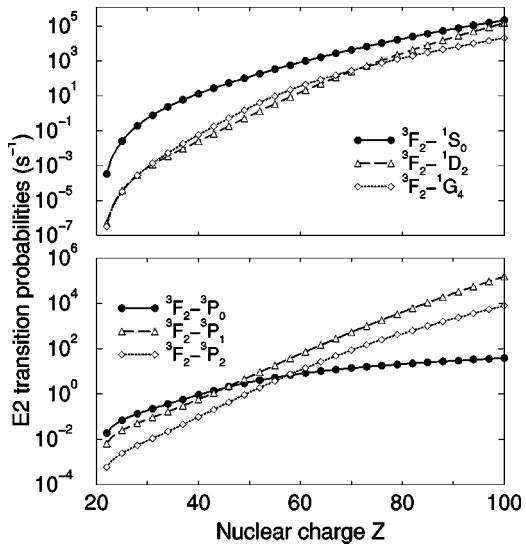

FIG. 7. Transition probabilities for LS allowed and forbidden electric quadrupole lines as functions of Z.

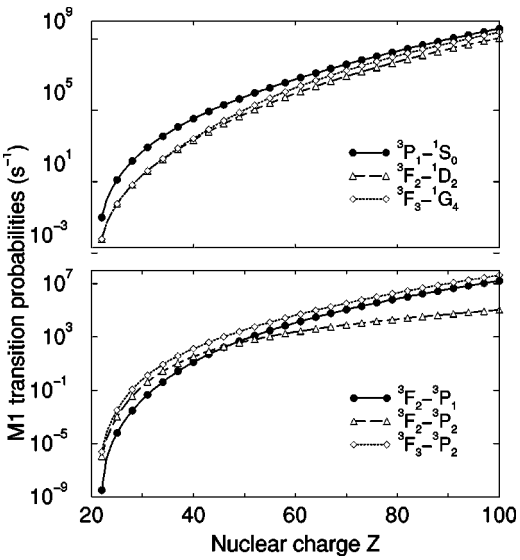

FIG. 8. Transition probabilities for magnetic dipole lines as functions of Z.

$$A^{E2}({}^3P_J - {}^3P_{J'}) \propto Z^{16}, \quad A^{E2}({}^3F_2 - {}^3F_{J'}) \propto Z^{16},$$

$$A^{E2}({}^3F_3 - {}^3F_4) \propto Z,$$

$$A^{M1}({}^3P_J - {}^3P_{J'}) \propto Z^{12}, \quad A^{M1}({}^3F_2 - {}^3F_3) \propto Z^{12},$$

$$A^{M1}({}^3F_3 - {}^3F_4) \propto Z^3.$$

As can be seen from Figs. 5 and 6, values of A^{E2} are smaller than values of A^{M1} by three to four orders of magnitude. The $E2$ and $M1$ rates for transitions between different terms (LS-$L'S'$) are presented in Figs. 7 and 8. There are no LS allowed $M1$ transitions except transitions inside of a multiplet. The $M1$ transitions shown in Fig. 8 are LS forbidden transitions: $\Delta L=2$ (lower panel) and $\Delta S=1$ (upper panel). Eigenvectors C_1^I or C_1^F [Eq. (2.1)] are $\propto \alpha^2 Z^3$ in this case. Taking into account that ΔE for these transitions are $\propto Z$, we obtain $A^{M1} \propto Z^9$. With increasing Z, ΔE is $\propto \alpha^2 Z^4$ and the Z dependence of A^{M1} is Z^{18}. As can be seen from Fig. 8, the value of A^{M1} for the $^3F_2$-$^3P_1$ transition changes by 15 orders of magnitude from $Z=22$ to $Z=100$. The transitions between ^3F and ^3P terms are LS allowed in the case of electric quadrupole transitions. These transitions are shown in the lower panel of Fig. 7. The A^{E2} value of the $^3F_2$-$^3P_0$ transition changes by three orders of magnitude from $Z=22$ to $Z=100$.

In Table VI, we present line strengths S for magnetic dipole lines in Ca-like ions with nuclear charges $Z=25$, 30, 40, 60, 80, and 100. Although these S-values are obtained in the intermediate coupling scheme, both LS and jj designations are given in the table. As can be seen, LS forbidden transitions with $\Delta S=1$ and $\Delta L=2$ with very small S values for $Z=25$ and 30 become allowed in jj coupling. The $^3F_2$-$^3P_2$ transition has the smallest S value among the transitions shown in Table VI. This LS forbidden transition re-

TABLE VI. Line strengths S for $M1$ transitions.

$[LS]$		$Z=25$	$Z=30$	$Z=40$	$Z=60$	$Z=80$	$Z=100$	$[jj]$	
$^3P_1$	$^1S_0$	7.31[−4]	6.14[−3]	6.74[−2]	4.21[−1]	6.31[−1]	7.03[−1]	$3d^*3d(1)$	$3d3d(0)$
$^3P_0$	$^3P_1$	2.00[0]	1.99[0]	1.93[0]	1.56[0]	1.34[0]	1.24[0]	$3d^*3d^*(0)$	$3d^*3d(1)$
$^3F_2$	$^3P_1$	1.24[−6]	8.02[−5]	4.53[−3]	5.27[−2]	8.79[−2]	1.02[−1]	$3d^*3d^*(2)$	$3d^*3d(1)$
$^1D_2$	$^3P_1$	5.93[−2]	3.27[−1]	8.79[−1]	1.19[0]	1.24[0]	1.26[0]	$3d^*3d(2)$	$3d^*3d(1)$
$^3P_1$	$^3P_2$	2.44[0]	2.17[0]	1.61[0]	1.25[0]	1.15[0]	1.11[0]	$3d^*3d(1)$	$3d3d(2)$
$^3F_2$	$^1D_2$	3.41[−3]	2.42[−2]	2.00[−1]	8.66[−1]	1.17[0]	1.26[0]	$3d^*3d^*(2)$	$3d^*3d(2)$
$^3F_2$	$^3P_2$	3.04[−5]	1.03[−3]	8.57[−3]	3.55[−3]	6.61[−4]	1.55[−4]	$3d^*3d^*(2)$	$3d3d(2)$
$^1D_2$	$^3P_2$	1.74[−1]	8.59[−1]	1.81[0]	2.22[0]	2.30[0]	2.30[0]	$3d^*3d(2)$	$3d3d(2)$
$^3F_3$	$^1D_2$	6.84[−3]	4.58[−2]	3.06[−1]	1.10[0]	1.46[0]	1.60[0]	$3d^*3d(3)$	$3d^*3d(2)$
$^3F_3$	$^3P_2$	1.12[−4]	4.40[−3]	7.41[−2]	2.97[−1]	3.96[−1]	4.30[−1]	$3d^*3d(3)$	$3d3d(2)$
$^3F_2$	$^3F_3$	6.66[0]	6.61[0]	6.27[0]	5.23[0]	4.73[0]	4.51[0]	$3d^*3d^*(2)$	$3d^*3d(3)$
$^3F_3$	$^3F_4$	6.75[0]	6.73[0]	6.50[0]	3.19[0]	1.87[0]	1.58[0]	$3d^*3d(3)$	$3d^*3d(4)$
$^3F_3$	$^1G_4$	1.38[−3]	1.27[−2]	2.29[−1]	3.52[0]	4.80[0]	5.03[0]	$3d^*3d(3)$	$3d3d(4)$
$^3F_4$	$^1G_4$	2.36[−3]	2.16[−2]	3.73[−1]	2.79[0]	2.22[0]	1.96[0]	$3d^*3d(4)$	$3d3d(4)$

TABLE VII. Lifetimes in seconds of $3d^2$ levels in Ca-like ions.

Z	$^3F_3$	$^3F_4$	$^1D_2$	$^3P_0$	$^3P_1$	$^3P_2$	$^1G_4$	$^1S_0$
26	3.42[+1]	2.35[+1]	2.51[+0]	1.12[+1]	8.76[+0]	5.07[+0]	2.84[+0]	4.34[−2]
28	5.88[+0]	4.39[+0]	5.91[−1]	7.46[+0]	4.34[+0]	1.27[+0]	6.42[−1]	2.30[−2]
32	3.32[−1]	3.05[−1]	6.97[−2]	3.75[+0]	9.17[−1]	8.87[−2]	6.52[−2]	5.28[−3]
36	3.26[−2]	3.83[−2]	1.34[−2]	2.00[+0]	1.53[−1]	1.02[−2]	1.07[−2]	1.14[−3]
42	1.93[−3]	3.68[−3]	1.69[−3]	8.20[−1]	9.20[−3]	7.93[−4]	1.09[−3]	1.52[−4]
47	2.82[−4]	9.52[−4]	3.57[−4]	4.22[−1]	1.08[−3]	1.38[−4]	1.92[−4]	3.70[−5]
54	2.99[−5]	3.33[−4]	4.98[−5]	2.02[−1]	8.54[−5]	1.75[−5]	2.13[−5]	6.68[−6]
62	3.61[−6]	1.94[−4]	6.90[−6]	1.11[−1]	8.14[−6]	2.37[−6]	2.62[−6]	1.21[−6]
74	2.71[−7]	1.13[−4]	5.63[−7]	5.99[−2]	5.04[−7]	1.94[−7]	2.05[−7]	1.29[−7]
83	5.32[−8]	6.92[−5]	1.14[−7]	4.26[−2]	9.13[−8]	3.94[−8]	4.10[−8]	2.95[−8]
92	1.26[−8]	2.99[−5]	2.75[−8]	3.19[−2]	2.06[−8]	9.55[−9]	9.83[−9]	7.73[−9]

mains forbidden also in the jj coupling scheme. The second-order contribution alone is responsible for the nonzero S value of the $3d_{3/2}3d_{3/2}$ (2)-$3d_{5/2}3d_{5/2}$ (2) transition.

In Table IV of the supplementary data set [24], MBPT results for $E2$ and $M1$ transitions probabilities between $3d^2$ levels are compared with results recently presented by Biémont *et al.* [11]. Differences range from 1% to 70% and decrease as Z increases.

C. Lifetimes in Ca-like ions

In Table VII, a subset of our MPBT data is presented for the nine $3d^2$ levels of Ca-like ions. The difference in the lifetimes of the individual multiplet levels increases when Z increases.

Contributions of different channels to the lifetimes of the $3d^2\,^1D_2$, and $3d^2\,^1S_0$ levels are shown in Fig. 9. The curves represent the ratios of individual transition probabilities A_k to the sum of all transition probabilities $\Sigma_k A_k$ for the level considered. It is seen from Fig. 9, that the largest contribution to the lifetime of the $3d^2\,^1D_2$ level is from $A^{M1}(^3F_{2,3} - {}^1D_2)$. Contributions of $E2$ channels are very small for all Z. The electric quadrupole transition is important for the lifetime of the $3d^2\,^1S_0$ level. As can be seen from Fig. 9, the contribution of $A^{E2}(^1D_2 - {}^1S_0)$ is dominant for small Z. For small Z, $A^{E2}(^3F_{2,3} - {}^3P_1)$ give the main contributions in the lifetime of the $3d^2\,^3P_1$ level. Only $A^{E2}(^3F_2 - {}^3P_0)$ contributes into the lifetime of the $3d^2\,^3P_0$ level. Magnetic dipole transitions give dominant contribution in the lifetime of the $3d^2\,^3F_{3,4}$, $^1G_4$, and $^3P_2$ levels.

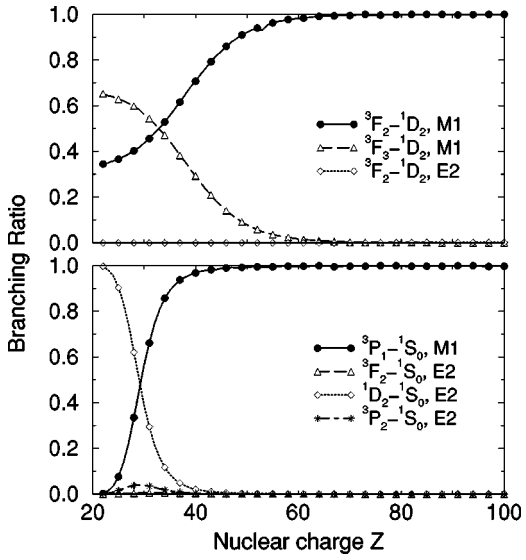

FIG. 9. Channel contribution to the $3d^2\,^1D_2$ and $3d^2\,^1S_0$ lifetimes as functions of Z.

IV. CONCLUSION

In summary, we present a systematic second-order relativistic MBPT study of energies, reduced matrix elements, line strengths, and transition rates for allowed and forbidden electric quadrupole and magnetic dipole transitions within the $3d^2$ multiplet for Ca-like ions with nuclear charges ranging from $Z=22$ to 100. The retarded dipole matrix elements include correlation corrections from Coulomb and Breit interactions. Contributions from negative-energy states were also included in the second-order matrix elements. Both length and velocity forms of the electric quadrupole matrix elements were evaluated, and small differences, caused by the nonlocality of the starting DF potential, were found between the two forms. Second-order MBPT transition energies were used to evaluate transition rates.

ACKNOWLEDGMENTS

The work of W.R.J. was supported in part by National Science Foundation Grant No. PHY-99-70666. U.I.S. acknowledges partial support by Grant No. B503968 from Lawrence Livermore National Laboratory.

APPENDIX A: ELECTRIC QUADRUPOLE MATRIX ELEMENT

The first-order reduced quadrupole matrix element $Z_2^{(1)}$ for the transition between two states $vw(J)-v'w'(J')$ is [18]

$$Z_2^{(1)}[v_1w_1(J)-v_2w_2(J')]$$
$$=\sqrt{[J][J']}\sum_{vw}\sum_{v'w'}\mathcal{S}^J(v_1w_1,vw)\mathcal{S}^{J'}(v_2w_2,v'w')$$
$$\times(-1)^{2+j_w+j_{v'}}\begin{Bmatrix} J & J' & 2\\ j_{v'} & j_w & j_v\end{Bmatrix}Z_2(v'w)\delta_{vw'}, \tag{A1}$$

where $[J]=2J+1$. The quantity $\mathcal{S}^J(v_1w_1,vw)$ is a symmetry coefficient defined by

$$\mathcal{S}^J(v_1w_1,vw)$$
$$=\eta_{v_1w_1}[\delta_{v_1v}\delta_{w_1w}+(-1)^{j_v+j_w+J+1}\delta_{v_1w}\delta_{w_1v}], \tag{A2}$$

where η_{vw} is a normalization factor given by

$$\eta_{vw}=\begin{cases}1 & \text{for } w\neq v\\ 1/\sqrt{2} & \text{for } w=v.\end{cases}$$

The electric quadrupole matrix element $Z_2(vw)$, which includes retardation, is given in velocity and length forms by Johnson *et al.* [27] where length form

$$Z_2(vw)=\langle\kappa_v\|C_2\|\kappa_w\rangle\frac{15}{k^2}\int_0^\infty dr\Bigg\{j_2(kr)[G_v(r)G_w(r)$$
$$+F_v(r)F_w(r)]+j_3(kr)\Bigg[\frac{\kappa_v-\kappa_w}{3}[G_v(r)F_w(r)$$
$$+F_v(r)G_w(r)]+[G_v(r)F_w(r)-F_v(r)G_w(r)]\Bigg]\Bigg\}, \tag{A3}$$

where velocity form

$$Z_2(vw)=\langle\kappa_v\|C_2\|\kappa_w\rangle\frac{15}{k^2}\int_0^\infty dr\Bigg\{2\frac{j_2(kr)}{kr}[G_v(r)F_w(r)$$
$$-F_v(r)G_w(r)]-\frac{\kappa_v-\kappa_w}{3}\Bigg[-j_3(kr)+\frac{3}{kr}j_2(kr)\Bigg]$$
$$\times[G_v(r)F_w(r)+F_v(r)G_w(r)]\Bigg\}. \tag{A4}$$

Second-order contributions to $E1$ reduced matrix elements are written out in Ref. [18]. It is only necessary to replace the quantities Z_{vw} in Ref. [18] by $Z_2(uw)$ Eqs. (A3) and (A4), to obtain the corresponding second-order contributions to $E2$ reduced matrix elements. The reduced matrix element for the derivative term is given by

$$Z^{(\mathrm{derv})}[vw(J)-v'w'(J')]$$
$$=\alpha\ (E_{vw}^{(1)}-E_{v'w'}^{(1)})P^{(\mathrm{derv})}[vw(J)-v'w'(J')], \tag{A5}$$

where $E_{vw}^{(1)}$, is the first-order correction to the energy given by Eqs. (2.8)–(2.10) of Ref. [15]. The quantity $P^{(\mathrm{derv})}$ introduced above is given by

$$P^{(\mathrm{derv})}[v_1w_1(J)-v_2w_2(J')]$$
$$=\sqrt{[J][J']}\sum_{vw}\sum_{v'w'}S^J(v_1w_1,vw)S^{J'}(v_2w_2,v'w')$$
$$\times(-1)^{1+j_w+j_{v'}}\begin{Bmatrix} J & J' & 1\\ j_{v'} & j_w & j_v\end{Bmatrix}Z_2^{(\mathrm{derv})}(v'w)\delta_{vw'}, \tag{A6}$$

where length form

$$Z_2^{(\mathrm{derv})}(vw)=\langle\kappa_v\|C_2\|\kappa_w\rangle\frac{15}{k^2}\int_0^\infty dr[2j_2(kr)-(kr)j_3(kr)]$$
$$\times[G_v(r)G_w(r)+F_v(r)F_w(r)]$$
$$+\langle\kappa_v\|C_2\|\kappa_w\rangle\frac{15}{k^2}\int_0^\infty dr[(kr)j_2(kr)-4j_3(kr)]$$
$$\times\Bigg\{\frac{\kappa_v-\kappa_w}{3}[G_v(r)F_w(r)+F_v(r)G_w(r)]$$
$$+[G_v(r)F_w(r)-F_v(r)G_w(r)]\Bigg\}, \tag{A7}$$

where velocity form

$$Z_2^{(\mathrm{derv})}(vw)=\langle\kappa_v\|C_2\|\kappa_w\rangle\frac{15}{k^2}\int_0^\infty dr\Bigg\{\Bigg[-2j_3(kr)+2\frac{j_2(kr)}{kr}\Bigg]$$
$$\times[G_v(r)F_w(r)-F_v(r)G_w(r)]$$
$$-\frac{\kappa_v-\kappa_w}{3}\Bigg[-(kr)j_2(kr)+j_3(kr)+\frac{3}{kr}j_2(kr)\Bigg]$$
$$\times[G_v(r)F_w(r)+F_v(r)G_w(r)]\Bigg\}. \tag{A8}$$

APPENDIX B: VELOCITY FORM OF THE $E2$ MATRIX ELEMENT

The second-order correlation contribution for $E2$ matrix element $Z^{(\mathrm{corr})}$ for transition between two states $vw(J)$ and $v'w'(J')$ is [19]

$$Z^{(\mathrm{corr})}[v_1w_1(J)-v_2w_2(J')]=\sqrt{[J][J']}\sum_{vw}\sum_{v'w'}S^J(v_1w_1,vw)S^{J'}(v_2w_2,v'w')\sum_k(-1)^{2+k}$$
$$\times\sum_i\left[\frac{Z_2(iv)X_k(v'w'wi)}{\epsilon_i+\epsilon_w-\epsilon_{v'}-\epsilon_{w'}}\begin{Bmatrix}J & J' & 2\\ j_i & j_v & j_w\end{Bmatrix}\begin{Bmatrix}j_i & j_w & J'\\ j_{v'} & j_{w'} & k\end{Bmatrix}(-1)^{J+j_w+j_{w'}}\right.$$
$$\left.+\frac{Z_2(v'i)X_k(iw'vw)}{\epsilon_i+\epsilon_{w'}-\epsilon_v-\epsilon_w}\begin{Bmatrix}J' & J & 1\\ j_i & j_{v'} & j_{w'}\end{Bmatrix}\begin{Bmatrix}j_i & j_{w'} & J\\ j_w & j_v & k\end{Bmatrix}(-1)^{j_v+j_{v'}}\right]. \quad \text{(B1)}$$

In the above equations, the index i denotes an arbitrary core or excited state. In the sum occurring in the first term of Eq. (B1), states i for which (iw) is in the model space of final states $(v'w')$ are excluded, while in the second term, states i for which (iw') is in the model space of initial states (vw) are excluded. We use $X_k(abcd)$ to denote a two-particle (Coulomb+Breit) interaction:

$$X_k(abcd)=\langle a||C_k||c\rangle\langle b||C_k||d\rangle R_k(abcd)\,. \quad \text{(B2)}$$

The quantities C_k are normalized spherical harmonics and $R_k(abcd)$ are Slater integrals. To include correlation corrections from the Breit interaction, the Coulomb matrix element $X_k(abcd)$ must be modified according to the rule:

$$X_k(abcd)\to X_k(abcd)+M_k(abcd)+N_k(abcd). \quad \text{(B3)}$$

The magnetic radial integrals M_k and N_k are defined by Eqs. (A4) and (A5) in Ref. [28].

In the case when $v_1w_1=v_2w_2$, we obtain

$$Z^{(\mathrm{corr})}[vw(J)-vw(J')]$$
$$=\sqrt{[J][J']}(-1)^{1+j_v+j_w}\left[\sum_{i\neq v}\frac{Z_2(iv)}{\epsilon_i-\epsilon_v}Y_{J'}(wvwi)\right.$$
$$\times\begin{Bmatrix}J & J' & 2\\ j_i & j_v & j_w\end{Bmatrix}(-1)^{J+1}+\sum_{i\neq v}\frac{Z_2(vi)}{\epsilon_i-\epsilon_v}Y_J(iwvw)$$
$$\times\begin{Bmatrix}J' & J & 2\\ j_i & j_v & j_w\end{Bmatrix}(-1)^{J+1}+\sum_{i\neq w}\frac{Z_2(iw)}{\epsilon_i-\epsilon_w}Y_{J'}(vwvi)$$
$$\times\begin{Bmatrix}J & J' & 2\\ j_i & j_w & j_v\end{Bmatrix}(-1)^{J'+1}+\sum_{i\neq w}\frac{Z_2(wi)}{\epsilon_i-\epsilon_w}Y_J(ivwv)$$
$$\left.\times\begin{Bmatrix}J' & J & 2\\ j_i & j_w & j_v\end{Bmatrix}(-1)^{J'+1}\right], \quad \text{(B4)}$$

where

$$Y_J(abcd)=\sum_k(-1)^{j_b+j_c+k}\left[X_k(abcd)\begin{Bmatrix}j_a & j_b & J\\ j_d & j_c & k\end{Bmatrix}(-1)^J\right.$$
$$\left.+X_k(abdc)\begin{Bmatrix}j_a & j_b & J\\ j_c & j_d & k\end{Bmatrix}\right]. \quad \text{(B5)}$$

The nonrelativistic limit for the velocity form of electric quadrupole matrix element $Z_2(vw)$ is

$$Z_2^{nr}(vw)=\frac{(\varepsilon_v-\varepsilon_w)}{\omega}Z(vw);$$

$$Z(vw)=\langle\kappa_v\|C_2\|\kappa_w\rangle\int_0^\infty dr\,r^2P_v(r)P_w(r). \quad \text{(B6)}$$

It is evident, that using this expression for $Z^{(\mathrm{corr})}$, we obtain in the nonrelativistic limit the following expression for this diagram in velocity form

$$Z^{(\mathrm{corr})}[vw(J)-vw(J')]$$
$$=\frac{1}{\omega}\sqrt{[J][J']}(-1)^{j_v+j_w}\times\left[Z(vv)(-1)^J\begin{Bmatrix}J & J' & 2\\ j_v & j_v & j_w\end{Bmatrix}\right.$$
$$\times[Y_{J'}(wvwv)-Y_J(vwvw)]+Z(ww)(-1)^{J'}$$
$$\left.\times\begin{Bmatrix}J & J' & 2\\ j_w & j_w & j_v\end{Bmatrix}[Y_{J'}(vwvw)-Y_J(wvwv)]\right]. \quad \text{(B7)}$$

Using the definition for first-order energy correction, Eq. (2.10) [15], we obtain the final expression for the contribution of the correlation diagram calculated in velocity form:

$$Z^{(\mathrm{corr})}[vw(J)-vw(J')]$$
$$=\frac{1}{\omega}[E_1^I-E_1^F]P^{(\mathrm{derv})}[vw(J)-vw(J')], \quad \text{(B8)}$$

where

$$P^{(\mathrm{derv})}[vw(J)-vw(J')]$$
$$=\sqrt{[J][J']}(-1)^{j_v+j_w}\left[Z(vv)(-1)^J\begin{Bmatrix}J & J' & 2\\ j_v & j_v & j_w\end{Bmatrix}\right.$$
$$\left.+Z(ww)(-1)^{J'}\begin{Bmatrix}J & J' & 2\\ j_w & j_w & j_v\end{Bmatrix}\right]. \quad \text{(B9)}$$

[1] G. A. Martin, J. R. Fuhr, and W. L. Wiese, J. Phys. Chem. Ref. Data Suppl. **17**, 3 (1988).
[2] J. R. Fuhr, G. A. Martin, and W. L. Wiese, J. Phys. Chem. Ref. Data Suppl. **17**, 4 (1988).
[3] J. Sugar and A. Musgrove, J. Phys. Chem. Ref. Data **19**, 527 (1990).
[4] B. Edlén, Phys. Scr. **T8**, 5 (1984).
[5] A. D. Thackeray, Mem. R. Astron. Soc. **83**, 1 (1977).
[6] J. O. Ekberg, Phys. Scr. **23**, 7 (1981).
[7] R. D. Cowan, *The Theory of Atomic Structure and Spectra* (University of California Press, Berkeley, 1981).
[8] B. Warner and R. C. Kirkpatrick, Mon. Not. R. Astron. Soc. **144**, 397 (1969).
[9] H. Nussbaumer and P. J. Storey, Astron. Astrophys. **113**, 21 (1982).
[10] J. F. Wyart, J. E. Raassen, and P. H. M. Uylings, Phys. Scr. **32**, 169 (1985).
[11] E. Biémont, J. E. Hansen, P. Quinet, and C. J. Zeippen, J. Phys. B **25**, 5029 (1992).
[12] I. P. Grant, B. J. McKenzie, P. H. Norrington, D. F. Mayers, and N. C. Pyper, Comput. Phys. Commun. **21**, 207 (1980).
[13] W. Eissner, M. Jones, and H. Nussbaumer, Comput. Phys. Commun. **8**, 270 (1974).
[14] H. Nussbaumer and P. J. Storey, Astron. Astrophys. **64**, 139 (1978).
[15] M. S. Safronova, W. R. Johnson, and U. I. Safronova, Phys. Rev. A **53**, 4036 (1996).
[16] M. S. Safronova, W. R. Johnson, and U. I. Safronova, J. Phys. B **30**, 2375 (1997).
[17] M. S. Safronova, W. R. Johnson, and U. I. Safronova, Phys. Scr. **T73**, 48 (1997).
[18] U. I. Safronova, W. R. Johnson, M. S. Safronova, and A. Derevianko, Phys. Scr. **59**, 286 (1999).
[19] U. I. Safronova, A. Derevianko, M. S. Safronova, and W. R. Johnson, J. Phys. B **32**, 3527 (1999).
[20] U. I. Safronova, W. R. Johnson, and A. Derevianko, Phys. Scr. **60**, 46 (1999).
[21] U. I. Safronova, W. R. Johnson, and M. S. Safronova, At. Data Nucl. Data Tables **69**, 183 (1998).
[22] U. I. Safronova, W. R. Johnson, and A. E. Livingston, Phys. Rev. A **60**, 996 (1999).
[23] U. I. Safronova, W. R. Johnson, and H. G. Berry, Phys. Rev. A **61**, 052503 (2000).
[24] See AIP Document No. E-PLRAAN-63-093103 including four tables: Table I: Comparison of the differences, $\Delta = E_{\text{theor.}} - E_{\text{expt.}}$ in cm^{-1}, from the present MBPT calculations (a) with those from the SST calculations of Ref. [11] (b). Table II: Comparison of energies (cm^{-1}) of $3d^2$ levels relative to the $3d^2\,{}^3F_2$ level in Ca-like ions: *a* present, *b* Ref. [1], *c* Ref. [2], *d* Ref. [3], *e* Ref. [25] and *f* Ref. [10]. Table III: The fine-structure splitting (cm^{-1}) of the $3d^2\,{}^3P$ term in Ca-like ions: *a* present, *b* Refs. [1] and [2]. Table IV: Comparison of the transition probabilities in s^{-1}, calculated by MBPT (a) and SST and HFR Ref. [11] (b) codes. This document may be retrieved via the EPAPS homepage (http://www.aip.org/pubservs/epaps.html) or from ftp.aip.org in the directory/ epaps/. See the EPAPS homepage for more information.
[25] G. J. van het Hof, J. O. Ekberg, and A. E. Nilson, Phys. Scr. **41**, 252 (1990).
[26] S. Suckewer, E. Hinnow, S. Cohen, M. Finkenthal, and K. Sato, Phys. Rev. A **26**, 1161 (1982).
[27] W. R. Johnson, D. R. Plante, and J. Sapirstein, Adv. At., Mol., Opt. Phys. **35**, 255 (1995).
[28] M. H. Chen, K. T. Cheng, and W. R. Johnson, Phys. Rev. A **47**, 3692 (1993).